iScience

CellPress

Article

The Hidden Control Architecture of Complex Brain Networks

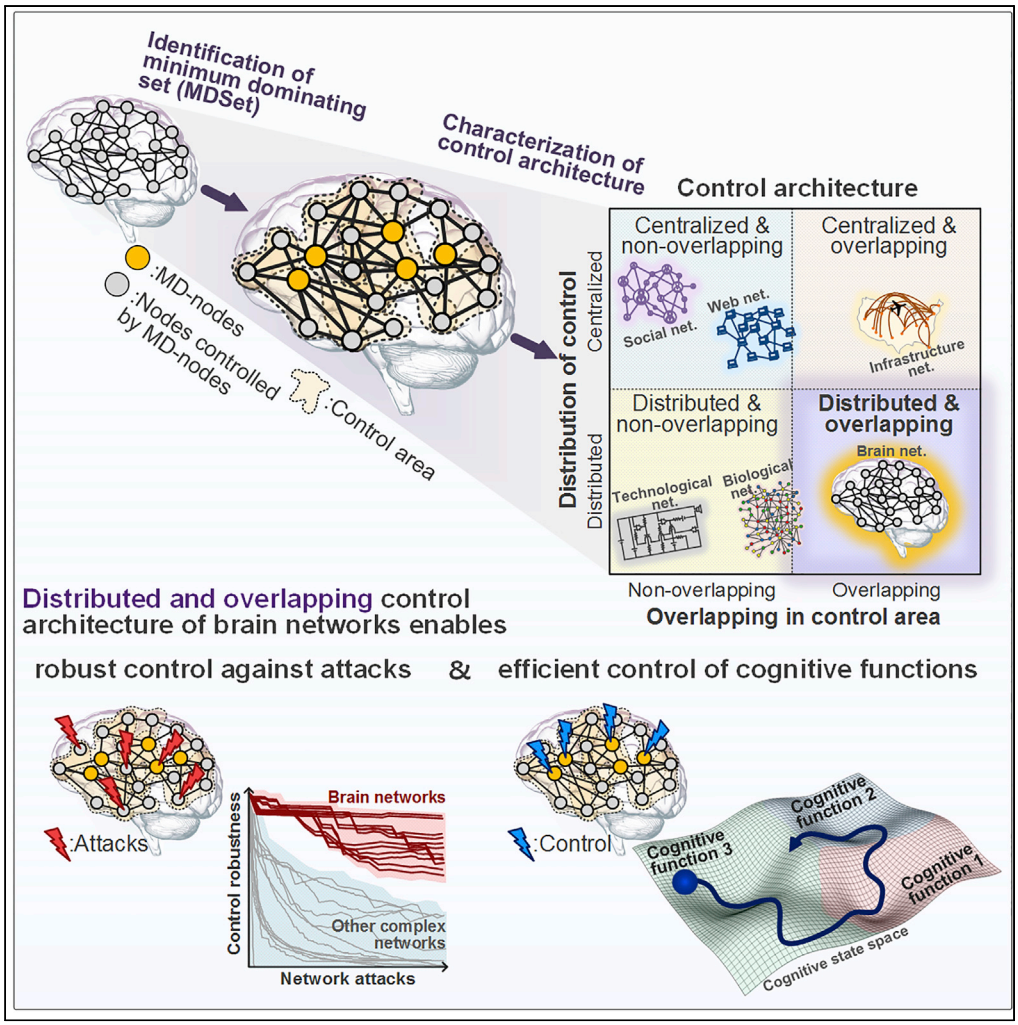

Byeongwook Lee, Uiryong Kang, Hongjun Chang, Kwang-Hyun Cho

ckh@kaist.ac.kr, http://sbie.kaist.ac.kr/

HIGHLIGHTS

We develop a framework to delineate the control architecture of brain networks

The control architecture of brain networks is compared with other complex networks

Brain networks have a distributed and overlapping control architecture

Robust and efficient brain functions might be rooted in its control architecture

Lee et al., iScience *13*, 154–162
March 29, 2019
https://doi.org/10.1016/j.isci.2019.02.017

iScience

CellPress

Article

The Hidden Control Architecture of Complex Brain Networks

Byeongwook Lee,[1] Uiryong Kang,[1] Hongjun Chang,[1] and Kwang-Hyun Cho[1,2,*]

SUMMARY

The brain controls various cognitive functions in a robust and efficient way. What is the control architecture of brain networks that enables such robust and optimal control? Is this brain control architecture distinct from that of other complex networks? Here, we developed a framework to delineate a control architecture of a complex network that is compatible with the behavior of the network and applied the framework to structural brain networks and other complex networks. As a result, we revealed that the brain networks have a *distributed and overlapping* control architecture governed by a small number of control nodes, which may be responsible for the robust and efficient brain functions. Moreover, our artificial network evolution analysis showed that the *distributed and overlapping* control architecture of the brain network emerges when it evolves toward increasing both robustness and efficiency.

INTRODUCTION

Cognitive functions are performed by the coordinated control of multiple brain regions (Cocchi et al., 2013; Ghazanfar and Schroeder, 2006; Koh et al., 2011). Such control is evolutionarily optimized for efficiency (Tang et al., 2017) and robustness (Aerts et al., 2016). Although such optimality is rooted in the complex interconnectivity of brain regions (Tang et al., 2017), our understanding of fundamental control architecture of brain networks that determines the specific coordinated control of interconnected brain regions is still lacking. Here, we investigated the control architecture of structural brain networks (hereafter, brain networks) by analyzing high-resolution brain networks reconstructed from multiple species, including fruit fly, nematode worm, mouse, cat, macaque, and human (Jarrell et al., 2012; Rubinov et al., 2015; Shih et al., 2015), and comparing them with 26 real-world complex networks. Our analysis included the reconstruction of brain networks of 100 healthy human adults (Figure 1A) to identify the control architecture of human brain networks. Using structural and diffusion magnetic resonance imaging (MRI) data obtained from Human Connectome Project, we performed whole-brain parcellation and diffusion tractography to identify the anatomical connections (i.e., edges) between 164 brain regions (i.e., nodes) extracted from the Destrieux atlas (Fischl et al., 2004) (Figure 1A, see Transparent Methods for details).

We developed a framework that determines the control architecture of complex networks on the basis of the minimum dominating set (MDSet) (Haynes et al., 1998), which refers to a minimal subset of nodes (MD-nodes) that control the remaining nodes through a one-step direct interaction (Figure 1B, see Transparent Methods). The important role of MD-nodes in network control is recognized both in theory (Nacher and Akutsu, 2012) and in various real-world networks (Nacher and Akutsu, 2013; Wan et al., 2002; Wuchty, 2014). In particular, the concept of MDSet has recently been adopted to analyze various biological networks, and the results showed that MD-nodes not only occupy strategic locations to control the networks but are also associated with various biological functions (Nacher and Akutsu, 2013, 2016; Sun, 2015; Wakai et al., 2017; Wuchty, 2014; Zhang et al., 2016). Thus, we postulated that the composition of MD-nodes in a network represents its hidden control architecture. By examining the MD-nodes in various complex networks, we delineated the distinct control architecture of each network, categorized the control architectures on the basis of the composition of MD-nodes in each network, and determined the attributes of each type of control architecture (Figure 1C). Through this process, we revealed the hidden control architecture of brain networks that is responsible for the efficient and robust control of brain functions.

RESULTS

Composition of Minimum Dominating Set in Brain Networks

We determined the MDSet of each network and compared the fraction of MD-nodes (M_D) of various networks. M_D is defined as the proportion of the size of MDSet to the size of the network and represents the

[1]Laboratory for Systems Biology and Bio-inspired Engineering, Department of Bio and Brain Engineering, Korea Advanced Institute of Science and Technology (KAIST), Daejeon 34141, Republic of Korea

[2]Lead Contact

*Correspondence: ckh@kaist.ac.kr, http://sbie.kaist.ac.kr/

https://doi.org/10.1016/j.isci.2019.02.017

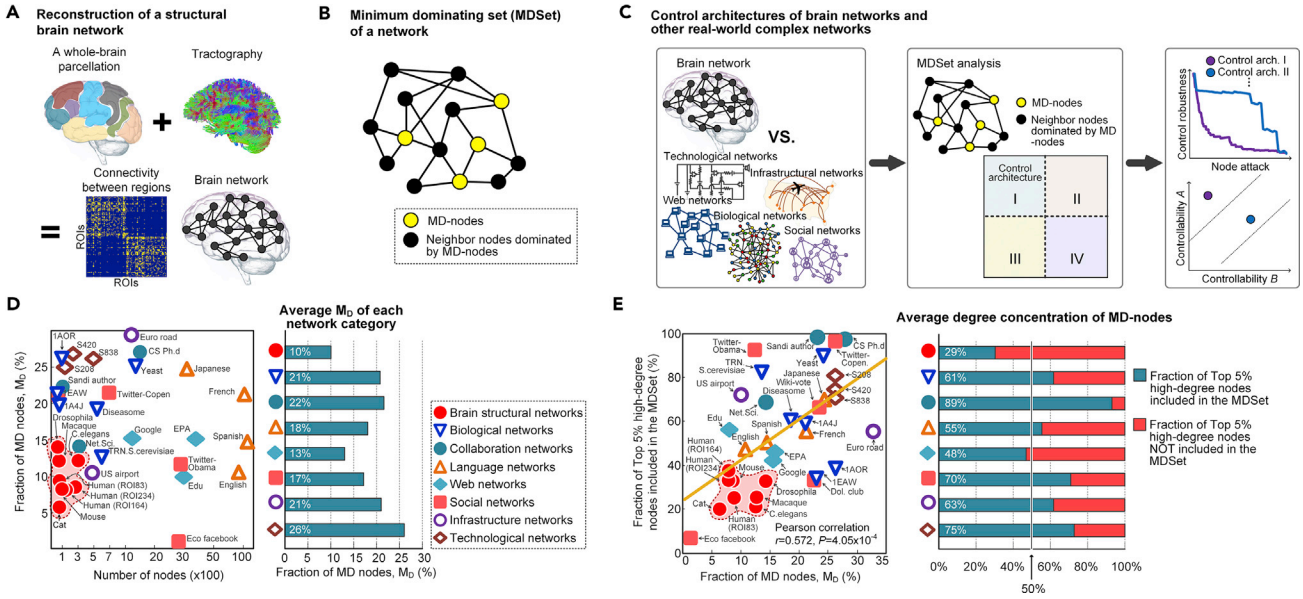

Figure 1. Comparison of Brain Networks and Other Real-World Complex Networks

(A) Schematic depicting the basic procedure of reconstructing a structural brain network (hereafter, brain network. See Transparent Methods for details).

(B) A minimum dominating set (MDSet) is defined as a minimal subset of nodes (yellow circle) with which all other remaining nodes (black circle) can be reached by one-step interactions.

(C) Schematic describing the overall framework of analysis. The control architectures of brain networks (*Caenorhabditis elegans*, *Drosophila*, mouse, cat, macaque, and human) and other real-world complex networks (26 networks of 7 categories) were characterized on the basis of their MDSet. By examining the composition of MD-nodes in each network, the control architecture of each network was categorized into a particular type. The attributes of each control architecture were then analyzed from various perspectives.

(D) Scatterplot comparing the fraction of MD-nodes, M_D, of various networks.

(E) Scatterplot showing the relationship between M_D and the proportion of high-degree nodes in the MDSet for each network (left, Pearson correlation $r = 0.572$, $p = 4.05 \times 10^{-4}$).

See also Figure S1.

minimum effort required to control the entire network (Nacher and Akutsu, 2012). We found that the average M_D of brain networks is lower than that of other networks (Figure 1D, see Table S1), implying that brain networks are optimized to minimize the control effort. High-degree nodes (nodes connected to many other nodes), especially highest-degree nodes, are more likely to be MD-nodes. Thus, we hypothesized that a network with low M_D would have MD-nodes that were enriched in high-degree nodes, which would result in a negative correlation between M_D and the proportion of high-degree nodes in the MDSet. To test this hypothesis, we investigated the relationship between the proportion of the top 5% high-degree nodes that are included in the MDSet and M_D. Unexpectedly, M_D and the proportion of high-degree nodes showed a positive correlation (Figure 1E, left, see Table S1). This positive correlation held when performed with the top 2%, 3%, 5%, 10%, 15%, and 20% of high-degree nodes (Figure S1), showing that this is a robust relationship. The proportion of high-degree nodes in the MDSets was more than 50% in most of the networks except brain networks, in which the proportion was much smaller (only 29% on average for eight brain networks, Figure 1E, right). This implied that the MD-nodes in brain networks are not solely determined by their degrees. Instead, they might be strategically placed and have a characteristic composition in the networks.

Identification of the Hidden Control Architecture of Brain Networks

To investigate the composition of MD-nodes in brain networks, we introduced two measures: *distribution of control (DC)* and *overlap in control area (OCA)*, where we define *DC* as the ratio of control area dominated by the MD-nodes in the top 5% high-degree nodes to that dominated by the rest of the MD-nodes, and we define *OCA* as the degree of overlap across all control areas among different MD-nodes (Figure 2A, left, see Transparent Methods). We tested various percentages (N = 5%–20%) of the top high-degree nodes and found that we could capture the particular control architecture of the brain networks that is distinct from other networks at N = 5% (Figure S2). Thus, we set $N = 5\%$ for the definition of *DC* measure.

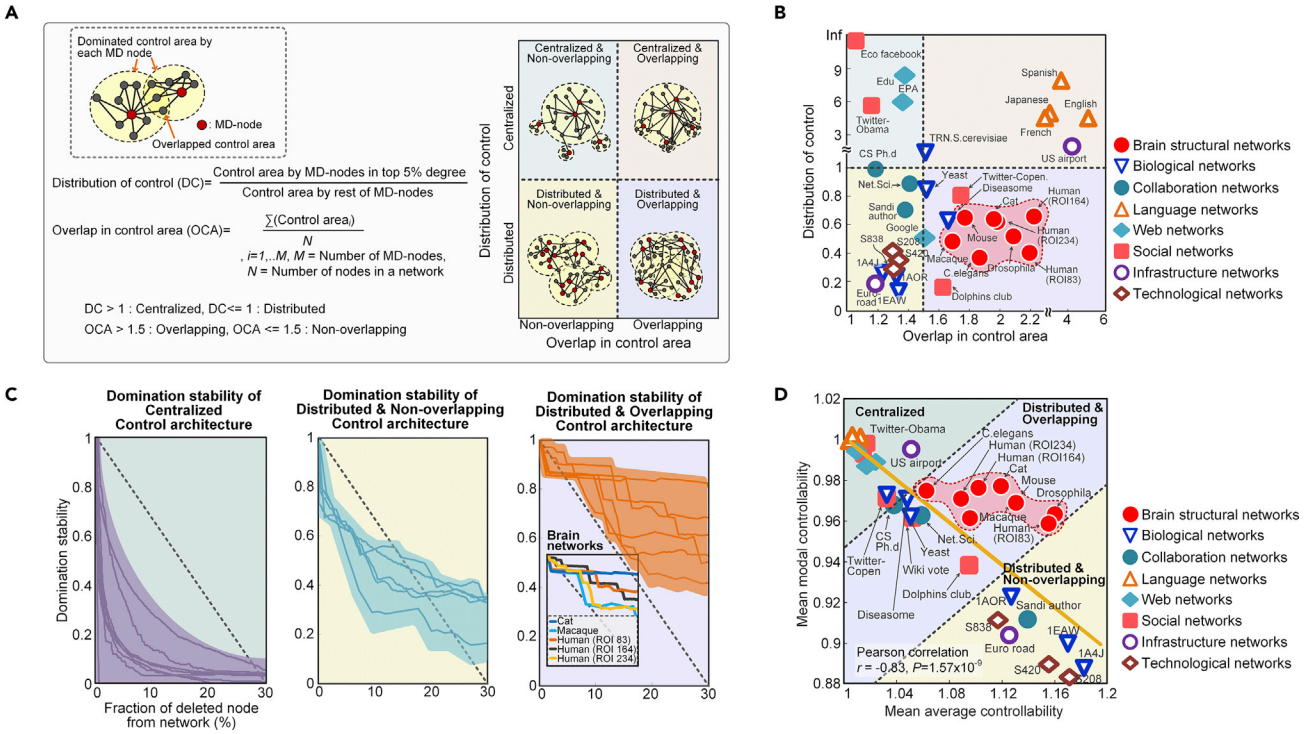

Figure 2. The Characteristics of Different Control Architectures

(A) Categorization of control architectures. On the basis of two measures, *distribution of control (DC)* and *overlap in control area (OCA)*, which determine the interdependence of control areas (measured by counting the number of nodes dominated by an MD-node, see Transparent Methods), the control architecture of a network can be categorized into four types. The background color indicates the type of different control architecture: blue for *centralized and non-overlapping* control architecture, pink for *centralized and overlapping* control architecture, yellow for *distributed and non-overlapping* control architecture, and purple for *distributed and overlapping* control architecture. The background color of the scatterplots in Figures 2B–2D indicates each type of control architecture described in Figure 2A.

(B) Scatterplot of *DC* versus *OCA* for each network. Using these two measures, each network can be categorized into a different type of control architecture. See also Figures S2 and S3.

(C) Domination stability of each control architecture under targeted attack. Disruption of control area along with the accumulated network damage was investigated for various networks (represented by each thin line). See also Figure S4.

(D) Scatterplot showing the mean modal controllability versus mean average controllability of various networks (Pearson correlation r = −0.83, p = 1.57 × 10^{-9}) and the underlying control architectures associated with controllability preference.

We defined networks with $DC > 1$ as centralized and $DC \leq 1$ as distributed. We confirmed the robustness of the classification by determining 100 MDSets for each network and computing the *DC* values of the corresponding MDSets (Figure S3A). We defined $OCA > 1.5$ as overlapping and $OCA \leq 1.5$ as non-overlapping and confirmed the robustness of this classification (Figure S3A). Using these two measures, we categorized the control architectures of various networks into four distinct types (Figure 2A, right). We found that all brain networks are categorized into one type, the *"distributed and overlapping"* control architecture (Figure 2B, see Table S1).

To further investigate whether this particular architecture is related to the robustness and efficiency of brain functioning, we examined the domination stability (Molnár et al., 2015) (see Transparent Methods), which reflects the robustness of the network to loss of nodes, of brain networks. Brain functions are robust against random attack (Hillary and Grafman, 2017), in biological terms, small, randomly occurring instances of neural injury or death or disruption in synaptic activity. Consequently, not all brain lesions have observable functional consequences. In contrast, damage of high-degree nodes, such as that caused by increased metabolic stress accompanied by high network burden, is associated with neurological disorders (Fornito et al., 2015), indicating that high-degree nodes represent vulnerabilities in the network with functional consequences to their disruption. Therefore, to measure domination stability we monitored the disruption of control area along with the network damage resulting from random attacks (Figure S4A) and targeted attacks that preferentially removed the highest-degree nodes (Figure S4B) in sequence to represent the

worst-case deterioration of network. In contrast to random attacks for which each type of network was robust (Figure S4A), each category of control architecture showed distinct domination stability to targeted attack of the highest-degree nodes (Figures 2C, S4B, and S4C). The *centralized* control architecture was the most fragile, showing a reduction in domination stability after removal of the fewest high-degree nodes (Figure 2C, left), whereas the *distributed and overlapping* control architecture showed the most robust stability and exhibited stair-like decrement against the sequential targeted attack (Figure 2C, right). We postulate that this property of *distributed and overlapping* control architecture might represent the robustness of brain functions despite deterioration of brain networks.

We also examined the controllability of different control architectures (see Transparent Methods). Here, controllability means the capability of driving a network state defined by a set of node activities into another one (Klamka, 1963). In particular, we considered mean *average controllability* and mean *modal controllability*, which describes the average ability to drive a network state into the easy-to-reach nearby state and that to drive into difficult-to-reach distant state, respectively (Gu et al., 2015) (see Transparent Methods). Under the previously known trade-off relationship between these two controllability measures (Tang et al., 2017), most of the networks showed a clear preference for either average or modal controllability (Figure 2D, see Table S1). Furthermore, such preference was associated with the underlying control architecture. For instance, networks with the *centralized* control architecture showed high mean modal controllability and low mean average controllability, whereas the networks with the *distributed and non-overlapping* control architecture showed the opposite. Notably, only the networks with the *distributed and overlapping* control architecture showed balanced controllability with respect to these two measures, indicating that the brain networks are optimized for both types of controllability.

The Structural Principle Underlying the Composition of MDSet in Brain Networks

Modern network science has revealed fundamental aspects of brain network organization, such as hierarchical modularity, hub nodes, and rich-club (RC)-nodes (Park and Friston, 2013; Sporns and Betzel, 2016; Van Den Heuvel and Sporns, 2011). RC-nodes function as connector hubs that determine inter-modular connectivity and are responsible for global integration (Van Den Heuvel and Sporns, 2011) (Figure 3A). We investigated whether MD-nodes have similar or distinct roles from RC-nodes and what kind of structural principles underlie the composition of MDSet. Therefore, we explored the MDSet of human brain networks with respect to modularity and RC organization of the networks (Figure 3A, see Transparent Methods). We found that the degree distribution of MD-nodes differs from that of RC-nodes (Figure 3B, left) and that only 38% of MD-nodes correspond to RC-nodes (Figure 3B, right).

Another type of hub node is the provincial hub node, which tends to have intra-modular connectivity (Sporns et al., 2007). Deletion of provincial hubs decreases network transitivity, measure reflecting the prevalence of clustered connectivity in the network (Sporns et al., 2007). We examined whether MD-nodes are provincial hubs by exploring the relationship between MD-nodes and network transitivity. We found that deletion of MD-nodes decreases the transitivity of networks (Figure 3C), indicating that many MD-nodes are provincial hub nodes. We further investigated the overall structural principle underlying the composition of MDSet by classifying MD-nodes into provincial nodes or connector nodes on the basis of their participation coefficients (Figure 3D, see Transparent Methods), a measure of a node's contribution to intra- or inter-modular connectivity. We found that the ratio of provincial to connector nodes is about 6:4 on average (Figure 3E). This means that about 60% MD-nodes are provincial nodes, which function as local controllers for segregated modules (that is execute distributed control), and the remaining MD-nodes function as global controllers for multiple modules (that is execute overlapping control). Thus, our results indicated that the MD-nodes constitute a *distributed and overlapping* control architecture of brain networks (Figure 3F). We explored whether this particular control architecture contributes to the optimal (i.e., balanced) controllability of brain networks with both effective average and modal controllability (Figure 2D). We selectively eliminated either provincial MD-nodes or connector MD-nodes from the network and assessed the effect on controllability (Figure 3G). We found that deletion of provincial MD-nodes reduces mean average controllability, whereas deletion of connector MD-nodes reduces mean modal controllability (Figure 3G, right). These results indicated that the combination of provincial and connector MD-nodes is a key structural characteristic resulting in the optimal controllability of brain networks.

The human ability to perform complex cognitive functions are rooted in the inter-regional brain network. In particular, previous neuroimaging studies revealed that subnetworks composed of different sets of brain

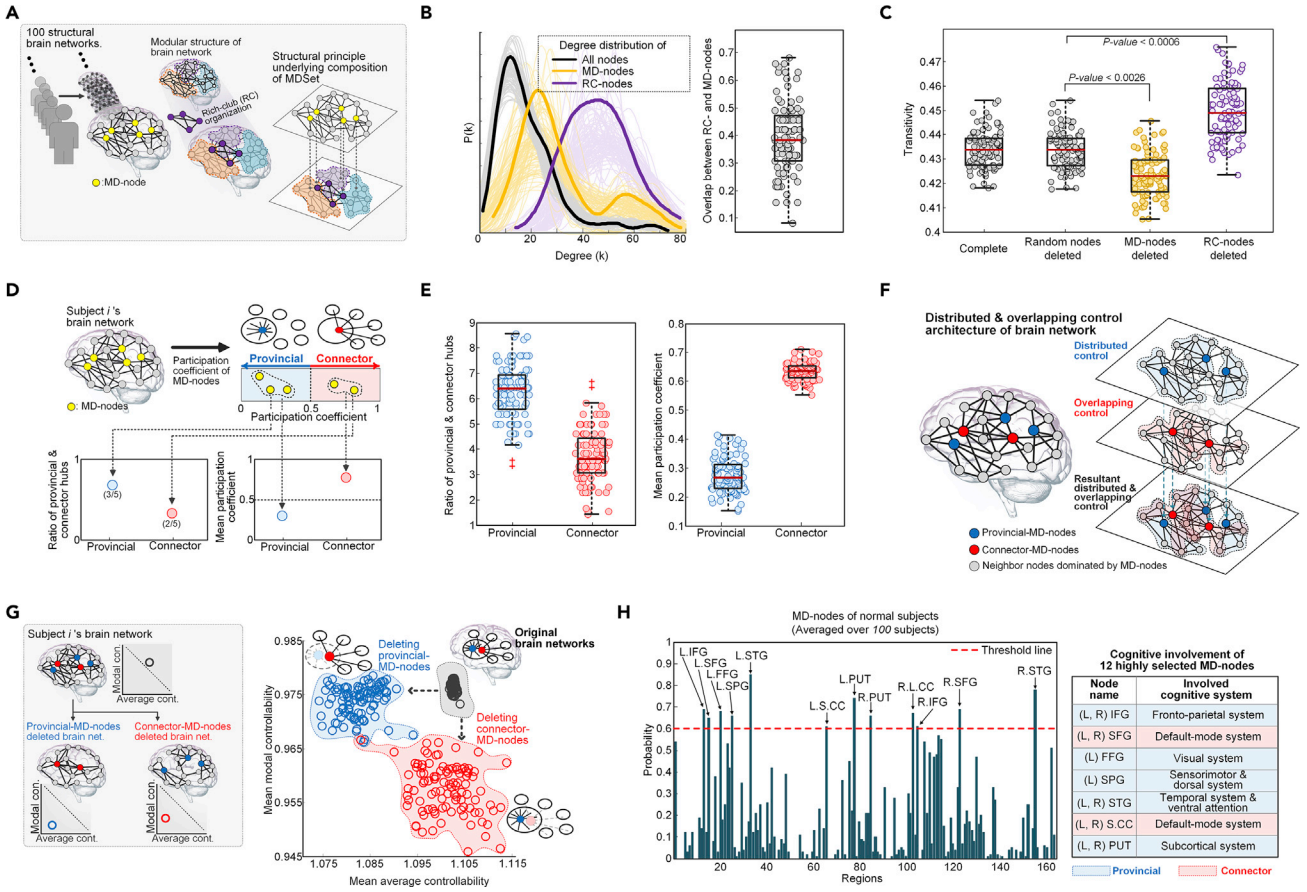

Figure 3. The Structural Principle Underlying the Composition of MDSet in Human Brain Networks

(A) Illustration of identifying MDSets from brain networks of 100 healthy adult subjects, composed of 164 cortical and subcortical regions extracted from the Destrieux atlas. The structural principle underlying the composition of MDSet is explored with respect to modularity and rich-club (RC) organization of the network.

(B) Degree distributions of all nodes, MD-nodes, and RC-nodes (left). The thin lines of black, yellow, and purple indicate the degree distributions of all nodes, MD-nodes, and RC-nodes of each network, respectively. The thick lines of black, yellow, and purple indicate the average of all thin lines of the same color. Comparison of MD-nodes and RC-nodes. Data are represented as box-and-whisker plot (right).

(C) Contribution of MD-nodes to the clustering capacity of each network is examined by the measure of *transitivity*. Data are represented as box-and-whisker plots.

(D) Participation coefficient (PC) values of MD-nodes are computed. MD-nodes are classified into either provincial or connector MD-nodes by their PC value (provincial if PC $\leq$ 0.5 and connector otherwise).

(E) Ratio of provincial to connector MD-nodes is computed. Data are represented as box-and-whisker plots.

(F) Illustration of the *distributed and overlapping* control architecture of brain networks that is formed by provincial and connector MD-nodes.

(G) Contribution of provincial- and connector-MD-nodes to determining the optimal (i.e., balanced) controllability of brain networks (left). Effect of elimination of provincial- and connector-MD-nodes on mean average controllability and mean modal controllability (right).

(H) Identification of the highly selected MD-nodes across 100 subjects. MD-nodes that are selected from more than 60% of the 100 subjects were chosen as the highly selected MD-nodes. Twelve nodes were chosen as the highly selected MD-nodes. FFG, fusiform gyrus; IFG, inferior frontal gyrus; PUT; putamen; S.CC, sulcus of corpus callosum; SFG, superior frontal gyrus; SPG, superior parietal gyrus; STG, superior temporal gyrus. Association of the highly selected MD nodes with the specific cognitive system (right).

regions are involved in carrying out distinct cognitive functions (Dosenbach et al., 2007; Power et al., 2011). These subnetworks are referred to as cognitive control networks or systems and commonly classified into visual, auditory, sensorimotor, attention, subcortical, frontoparietal, cingulo-opercular, and default-mode system (Power et al., 2011). From a cognitive perspective, the control of each cognitive system is important for implementing distinct cognitive functions and for a smooth transition between them. To explore the relationship between MD-nodes and cognitive functions, we chose the 12 MD-nodes, representing specific regions of the brain that are highly selected across subjects (Figure 3H, left), and examined whether the selected 12 bihemispheric regions are differently located in or between the cognitive systems. We found

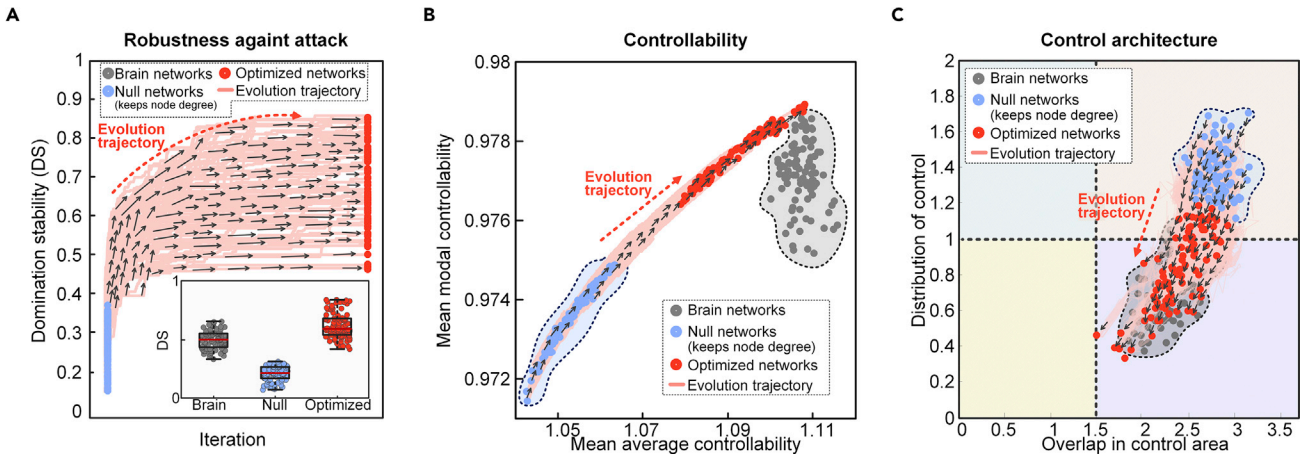

Figure 4. Exploring the Development of Control Architecture by Artificial Network Evolution

(A–C) We generated 100 degree-preserved random null networks (blue circles) derived from 100 structural human brain networks composed of 164 nodes (gray circles). Each colored circle represents an individual network. Starting from the generated random null networks, we performed artificial network evolution on each network by employing Pareto optimization to advance the following objective functions: (A) domination stability against targeted attack of top 20% high-degree nodes; (B) mean average controllability and mean modal controllability. Pink line in each figure indicates an evolution trajectory of each random null network, and red circles represent the pareto-optimal networks after the artificial evolution. (C) As the evolution proceeds, the control architecture of networks was transformed from a *centralized and overlapping* control architecture to the *distributed and overlapping* control architecture. See also Figure S5.

that each MD-node is differently associated with the cognitive system, suggesting that MD-nodes play a central role in controlling distinct cognitive functions (Figure 3H, right. See Table S2 for details). In particular, by classifying the MD-nodes into provincial or connector nodes, we found that provincial MD-nodes are associated with specialized cognitive control systems, such as the visual, sensorimotor, attention system, whereas the connector MD-nodes are associated with the default-mode system that enables the brain to move smoothly between different cognitive functions. These results indicate that MD-nodes might occupy strategic locations in the brain networks to control the cognitive functions.

Exploring the Development of Control Architecture by Artificial Network Evolution

We found that the brain networks have a *distributed and overlapping* control architecture and such a control architecture provides enhanced robustness (Figure 2C) and optimal (i.e., balanced) controllability (Figure 2D). To examine the relationship between structure and functional characteristics, we performed artificial network evolution starting from random null networks derived from the human brain networks and investigated robustness, controllability, and the corresponding control architectures along with evolution trajectories (Figure S5, see Transparent Methods for details). For this purpose, we first compared the following three features of the random null networks and the brain networks: domination stability against targeted attack of top 20% high-degree nodes, mean average controllability, and mean modal controllability (see Transparent Methods). As a result, we found that random null networks have much lower robustness and controllability than the brain networks (Figures 4A and 4B, and see Figure S5 for details). Moreover, random null networks have a *centralized and overlapping* control architecture in contrast with brain networks (Figures 4C and S5).

Starting from the random null networks, we performed artificial network evolution by employing Pareto optimization (Holland and Goldberg, 1989) in the direction of increasing the aforementioned three features (domination stability, mean average controllability, and mean modal controllability). Each evolutionary epoch was performed by carrying out two steps: network variation and network selection (see Transparent Methods for details). We generated randomly rewired networks, then we chose one that most advances the three features and used it in the next evolutionary epoch. Intriguingly, the artificial evolution trajectories that increase robustness and controllability (Figures 4A and 4B) lead to the *distributed and overlapping* control architecture (Figure 4C), implying that such a control architecture of the brain network might have emerged during evolution toward increasing both robustness and efficiency.

DISCUSSION

In many cases, efficiency and robustness are often regarded as having a trade-off relationship. However, the brain unusually exhibits both attributes when it performs complex cognitive functions. Such optimality must be rooted in a specific coordinated control of interconnected brain regions, but our understanding of the intrinsic control architecture of complex brain networks is still lacking. In this study, we investigated the intrinsic control architecture of structural brain networks of various species and compared them with the control architectures of other biological and man-made (e.g., social, infrastructural, technological) complex networks. In particular, we developed a framework for analyzing the control architecture of complex networks based on the minimum dominating set (MDSet), which refers to a minimal subset of nodes (MD-nodes) that control remaining nodes with one-step direct interaction.

Here, by exploring and comparing the structural principles underlying the composition of MDSets of various complex networks, we delineated their distinct control architectures. Interestingly, we found that the proportion of MDSet in brain networks is remarkably smaller compared with other complex networks (Figure 1D), implying that brain networks may have been optimized to minimize the control cost. Furthermore, we found that the MDSet of brain networks is not solely determined by the degree of nodes but rather strategically placed to form a particular control architecture (Figure 1E). Consequently, we revealed the hidden control architecture of brain networks, namely, *distributed and overlapping* control architecture that is distinct from other complex networks (Figure 2B). We found that such a particular control architecture brings about robustness against targeted attack (i.e., preferential attack on high-degree nodes, Figure 2C), which might be a fundamental basis of the robust brain functions against preferential damages of high-degree nodes (i.e., brain regions) (Fornito et al., 2015). Moreover, we found that the particular control architecture of brain networks also enables high efficiency in switching from one network state (defined by a set of node activities) to another (Figure 2D), a capability that is crucial for traversing diverse cognitive states. Lastly, our artificial network evolution analysis showed that the *distributed and overlapping* control architecture of the brain network emerges when it evolves toward increasing both robustness and efficiency (Figure 4). Taken together, our results suggest that the *distributed and overlapping* control architecture of brain networks might be responsible for the robust and efficient control of brain functions.

A variety of biological processes are determined by the underlying regulatory networks (Assmus et al., 2006; Dubitzky et al., 2013; Eshaghi et al., 2010; Kim and Cho, 2006; Kim et al., 2011; Kwon and Cho, 2007; Lee et al., 2018; Murray et al., 2010; Park et al., 2006; Shin et al., 2006; Sreenath et al., 2008) and disruption of the networks can lead to diverse biological disorders (Shin et al., 2014, 2017; Yeo et al., 2018). Hence, control of a biological network has become an important issue to systematically regulate or modulate biological processes at a network level (Kim et al., 2013; Wolkenhauer et al., 2004). Likewise, there is a growing interest in brain network control (Bassett and Sporns, 2017), and various control strategies were suggested (Betzel et al., 2016; Gu et al., 2015; Khambhati et al., 2016; Yan et al., 2017) with the aim of developing therapeutics (Braun et al., 2018) and methods for cognitive enhancement (Kenett et al., 2018). It is, however, essential to understand the inherent control architecture of brain networks before applying any external interventions, because the brain itself is already an autonomously controlled system. Our study revealed an intrinsic control architecture of brain networks that not only sheds light on the intrinsic control properties of a normal brain but also provides a basis for exogenous control of brain networks to address altered control architectures of various neurological disorders.

Limitations of the Study

In this study, we performed tractography and constructed structural brain networks (i.e., connectome) of 100 healthy human adults to investigate the control architecture of the human brain networks. Yet, there exist inherent limitations in the current tractography algorithms (Daducci et al., 2016; Jbabdi and Johansen-Berg, 2011; Jones and Cercignani, 2010). Briefly, current tractography algorithms can yield false-positive and false-negative connections, and in consequence, genuine connections might be detected invalid and spurious ones as plausible. Accordingly, biased or inaccurate conclusions can be drawn from missing or duplicated connections. These limitations have motivated ongoing technical improvement of tractography algorithms and development of connectome validation standards.

METHODS

All methods can be found in the accompanying Transparent Methods supplemental file.

SUPPLEMENTAL INFORMATION

Supplemental Information can be found online at https://doi.org/10.1016/j.isci.2019.02.017.

ACKNOWLEDGMENTS

We thank Nancy R. Gough (BioSerendipity, LLC) for editorial assistance. This work was supported by the National Research Foundation of Korea (NRF) grants funded by the Korea Government, the Ministry of Science, and ICT (2017R1A2A1A17069642 and 2015M3A9A7067220).

AUTHOR CONTRIBUTIONS

K.-H.C. designed the project and supervised the study. B. L. and K.-H.C. designed experiments and wrote the paper; B. L., U.K., and H.C. performed experiments and analyzed data; K.-H.C. obtained funding.

DECLARATION OF INTERESTS

The authors declare no competing interests.

Received: October 30, 2018
Revised: January 11, 2019
Accepted: February 15, 2019
Published: March 29, 2019

REFERENCES

Aerts, H., Fias, W., Caeyenberghs, K., and Marinazzo, D. (2016). Brain networks under attack: robustness properties and the impact of lesions. Brain *139*, 3063–3083.

Assmus, H.E., Herwig, R., Cho, K.-H., and Wolkenhauer, O. (2006). Dynamics of biological systems: role of systems biology in medical research. Expert Rev. Mol. Diagn. *6*, 891–902.

Bassett, D.S., and Sporns, O. (2017). Network neuroscience. Nat. Neurosci. *20*, 353.

Betzel, R.F., Gu, S., Medaglia, J.D., Pasqualetti, F., and Bassett, D.S. (2016). Optimally controlling the human connectome: the role of network topology. Sci. Rep. *6*, 30770.

Braun, U., Schaefer, A., Betzel, R.F., Tost, H., Meyer-Lindenberg, A., and Bassett, D.S. (2018). From maps to multi-dimensional network mechanisms of mental disorders. Neuron *97*, 14–31.

Cocchi, L., Zalesky, A., Fornito, A., and Mattingley, J.B. (2013). Dynamic cooperation and competition between brain systems during cognitive control. Trends Cogn. Sci. *17*, 493–501.

Daducci, A., Dal Palú, A., Descoteaux, M., and Thiran, J.-P. (2016). Microstructure informed tractography: pitfalls and open challenges. Front. Neurosci. *10*, 247.

Dosenbach, N.U., Fair, D.A., Miezin, F.M., Cohen, A.L., Wenger, K.K., Dosenbach, R.A., Fox, M.D., Snyder, A.Z., Vincent, J.L., and Raichle, M.E. (2007). Distinct brain networks for adaptive and stable task control in humans. Proc. Natl. Acad. Sci. U S A *104*, 11073–11078.

Dubitzky, W., Wolkenhauer, O., Yokota, H., and Cho, K.-H. (2013). Encyclopedia of Systems Biology (Springer Publishing Company, Incorporated).

Eshaghi, M., Lee, J.H., Zhu, L., Poon, S.Y., Li, J., Cho, K.-H., Chu, Z., Karuturi, R.K.M., and Liu, J. (2010). Genomic binding profiling of the fission yeast stress-activated MAPK Sty1 and the bZIP transcriptional activator Atf1 in response to H2O2. PLoS One *5*, e11620.

Fischl, B., Van Der Kouwe, A., Destrieux, C., Halgren, E., Ségonne, F., Salat, D.H., Busa, E., Seidman, L.J., Goldstein, J., and Kennedy, D. (2004). Automatically parcellating the human cerebral cortex. Cereb. Cortex *14*, 11–22.

Fornito, A., Zalesky, A., and Breakspear, M. (2015). The connectomics of brain disorders. Nat. Rev. Neurosci. *16*, 159.

Ghazanfar, A.A., and Schroeder, C.E. (2006). Is neocortex essentially multisensory? Trends Cogn. Sci. *10*, 278–285.

Gu, S., Pasqualetti, F., Cieslak, M., Telesford, Q.K., Alfred, B.Y., Kahn, A.E., Medaglia, J.D., Vettel, J.M., Miller, M.B., and Grafton, S.T. (2015). Controllability of structural brain networks. Nat. Commun. *6*, 8414.

Haynes, T.W., Hedetniemi, S., and Slater, P. (1998). Fundamentals of Domination in Graphs (CRC Press).

Hillary, F.G., and Grafman, J.H. (2017). Injured brains and adaptive networks: the benefits and costs of hyperconnectivity. Trends Cogn. Sci. *21*, 385–401.

Holland, J., and Goldberg, D. (1989). Genetic Algorithms in Search, Optimization and Machine Learning (Addison-Wesley).

Jarrell, T.A., Wang, Y., Bloniarz, A.E., Brittin, C.A., Xu, M., Thomson, J.N., Albertson, D.G., Hall, D.H., and Emmons, S.W. (2012). The connectome of a decision-making neural network. Science *337*, 437–444.

Jbabdi, S., and Johansen-Berg, H. (2011). Tractography: where do we go from here? Brain Connect. *1*, 169–183.

Jones, D.K., and Cercignani, M. (2010). Twenty-five pitfalls in the analysis of diffusion MRI data. NMR Biomed. *23*, 803–820.

Kenett, Y.N., Medaglia, J.D., Beaty, R.E., Chen, Q., Betzel, R.F., Thompson-Schill, S.L., and Qiu, J. (2018). Driving the brain towards creativity and intelligence: a network control theory analysis. Neuropsychologia *118* (Pt A), 79–90.

Khambhati, A.N., Davis, K.A., Lucas, T.H., Litt, B., and Bassett, D.S. (2016). Virtual cortical resection reveals push-pull network control preceding seizure evolution. Neuron *91*, 1170–1182.

Kim, J.-R., and Cho, K.-H. (2006). The multi-step phosphorelay mechanism of unorthodox two-component systems in E. coli realizes ultrasensitivity to stimuli while maintaining robustness to noises. Comput. Biol. Chem. *30*, 438–444.

Kim, J.-R., Kim, J., Kwon, Y.-K., Lee, H.-Y., Heslop-Harrison, P., and Cho, K.-H. (2011). Reduction of complex signaling networks to a representative kernel. Sci. Signal. *4*, ra35.

Kim, J., Park, S.-M., and Cho, K.-H. (2013). Discovery of a kernel for controlling biomolecular regulatory networks. Sci. Rep. *3*, 2223.

Kalman, R.E., Ho, Y., and Narendra, K.S. (1963). Controllability of Linear Dynamical Systems, Volume 1 of Contributions to Differential Equations (Wiley).

Koh, Y., Shin, K.S., Kim, J.S., Choi, J.-S., Kang, D.-H., Jang, J.H., Cho, K.-H., O'Donnell, B.F., Chung, C.K., and Kwon, J.S. (2011). An MEG study of alpha modulation in patients with schizophrenia and in subjects at high risk of developing psychosis. Schizophr. Res. *126*, 36–42.

Kwon, Y.-K., and Cho, K.-H. (2007). Boolean dynamics of biological networks with multiple coupled feedback loops. Biophys. J. *92*, 2975–2981.

Lee, B., Shin, D., Gross, S.P., and Cho, K.-H. (2018). Combined positive and negative feedback allows modulation of neuronal oscillation frequency during sensory processing. Cell Rep. *25*, 1548–1560.e3.

Molnár, F., Jr., Derzsy, N., Szymanski, B.K., and Korniss, G. (2015). Building damage-resilient dominating sets in complex networks against random and targeted attacks. Sci. Rep. *5*, 8321.

Murray, P.J., Kang, J.-W., Mirams, G.R., Shin, S.-Y., Byrne, H.M., Maini, P.K., and Cho, K.-H. (2010). Modelling spatially regulated β-catenin dynamics and invasion in intestinal crypts. Biophys. J. *99*, 716–725.

Nacher, J.C., and Akutsu, T. (2012). Dominating scale-free networks with variable scaling exponent: heterogeneous networks are not difficult to control. New J. Phys. *14*, 073005.

Nacher, J.C., and Akutsu, T.. (2013). Analysis on critical nodes in controlling complex networks using dominating sets. Paper presented at: Signal-Image Technology & Internet-Based Systems (SITIS), 2013 International Conference on (IEEE).

Nacher, J.C., and Akutsu, T. (2016). Minimum dominating set-based methods for analyzing biological networks. Methods *102*, 57–63.

Park, H.-J., and Friston, K. (2013). Structural and functional brain networks: from connections to cognition. Science *342*, 1238411.

Park, S.G., Lee, T., Kang, H.Y., Park, K., Cho, K.-H., and Jung, G. (2006). The influence of the signal dynamics of activated form of IKK on NF-κB and anti-apoptotic gene expressions: a systems biology approach. FEBS Lett. *580*, 822–830.

Power, J.D., Cohen, A.L., Nelson, S.M., Wig, G.S., Barnes, K.A., Church, J.A., Vogel, A.C., Laumann, T.O., Miezin, F.M., and Schlaggar, B.L. (2011). Functional network organization of the human brain. Neuron *72*, 665–678.

Rubinov, M., Ypma, R.J., Watson, C., and Bullmore, E.T. (2015). Wiring cost and topological participation of the mouse brain connectome. Proc. Natl. Acad. Sci. U S A *112*, 10032–10037.

Shih, C.-T., Sporns, O., Yuan, S.-L., Su, T.-S., Lin, Y.-J., Chuang, C.-C., Wang, T.-Y., Lo, C.-C., Greenspan, R.J., and Chiang, A.-S. (2015). Connectomics-based analysis of information flow in the Drosophila brain. Curr. Biol. *25*, 1249–1258.

Shin, D., Kim, I.S., Lee, J.M., Shin, S.-Y., Lee, J.-H., Baek, S.H., and Cho, K.-H. (2014). The hidden switches underlying ROR α-mediated circuits that critically regulate uncontrolled cell proliferation. J. Mol. Cell Biol. *6*, 338–348.

Shin, D., Lee, J., Gong, J.-R., and Cho, K.-H. (2017). Percolation transition of cooperative mutational effects in colorectal tumorigenesis. Nat. Commun. *8*, 1270.

Shin, S.-Y., Choo, S.-M., Kim, D., Baek, S.J., Wolkenhauer, O., and Cho, K.-H. (2006). Switching feedback mechanisms realize the dual role of MCIP in the regulation of calcineurin activity. FEBS Lett. *580*, 5965–5973.

Sporns, O., and Betzel, R.F. (2016). Modular brain networks. Annu. Rev. Psychol. *67*, 613–640.

Sporns, O., Honey, C.J., and Kötter, R. (2007). Identification and classification of hubs in brain networks. PLoS One *2*, e1049.

Sreenath, S.N., Cho, K.-H., and Wellstead, P. (2008). Modelling the dynamics of signalling pathways. Essays Biochem. *45*, 1–28.

Sun, P.G. (2015). Co-controllability of drug-disease-gene network. New J. Phys. *17*, 085009.

Tang, E., Giusti, C., Baum, G.L., Gu, S., Pollock, E., Kahn, A.E., Roalf, D.R., Moore, T.M., Ruparel, K., and Gur, R.C. (2017). Developmental increases in white matter network controllability support a growing diversity of brain dynamics. Nat. Commun. *8*, 1252.

Van Den Heuvel, M.P., and Sporns, O. (2011). Rich-club organization of the human connectome. J. Neurosci. *31*, 15775–15786.

Wakai, R., Ishitsuka, M., Kishimoto, T., Ochiai, T., and Nacher, J.C. (2017). Identification of genes and critical control proteins associated with inflammatory breast cancer using network controllability. PLoS One *12*, e0186353.

Wan, P.-J., Alzoubi, K.M., and Frieder, O.. (2002). Distributed construction of connected dominating set in wireless ad hoc networks. Paper presented at: INFOCOM 2002 Twenty-First annual joint conference of the IEEE computer and communications societies Proceedings IEEE (IEEE).

Wolkenhauer, O., Ghosh, B.K., and Cho, K.-H. (2004). Control and coordination in biochemical networks. IEEE Control Syst. Mag. *24*, 30–34.

Wuchty, S. (2014). Controllability in protein interaction networks. Proc. Natl. Acad. Sci. U S A *111*, 7156–7160.

Yan, G., Vértes, P.E., Towlson, E.K., Chew, Y.L., Walker, D.S., Schafer, W.R., and Barabási, A.-L. (2017). Network control principles predict neuron function in the *Caenorhabditis elegans* connectome. Nature *550*, 519–523.

Yeo, S.-Y., Lee, K.-W., Shin, D., An, S., Cho, K.-H., and Kim, S.-H. (2018). A positive feedback loop bi-stably activates fibroblasts. Nat. Commun. *9*, 3016.

Zhang, X.-F., Ou-Yang, L., Dai, D.-Q., Wu, M.-Y., Zhu, Y., and Yan, H. (2016). Comparative analysis of housekeeping and tissue-specific driver nodes in human protein interaction networks. BMC Bioinformatics *17*, 358.

ISCI, Volume *13*

Supplemental Information

The Hidden Control Architecture of Complex Brain Networks

Byeongwook Lee, Uiryong Kang, Hongjun Chang, and Kwang-Hyun Cho

Supplemental Figures

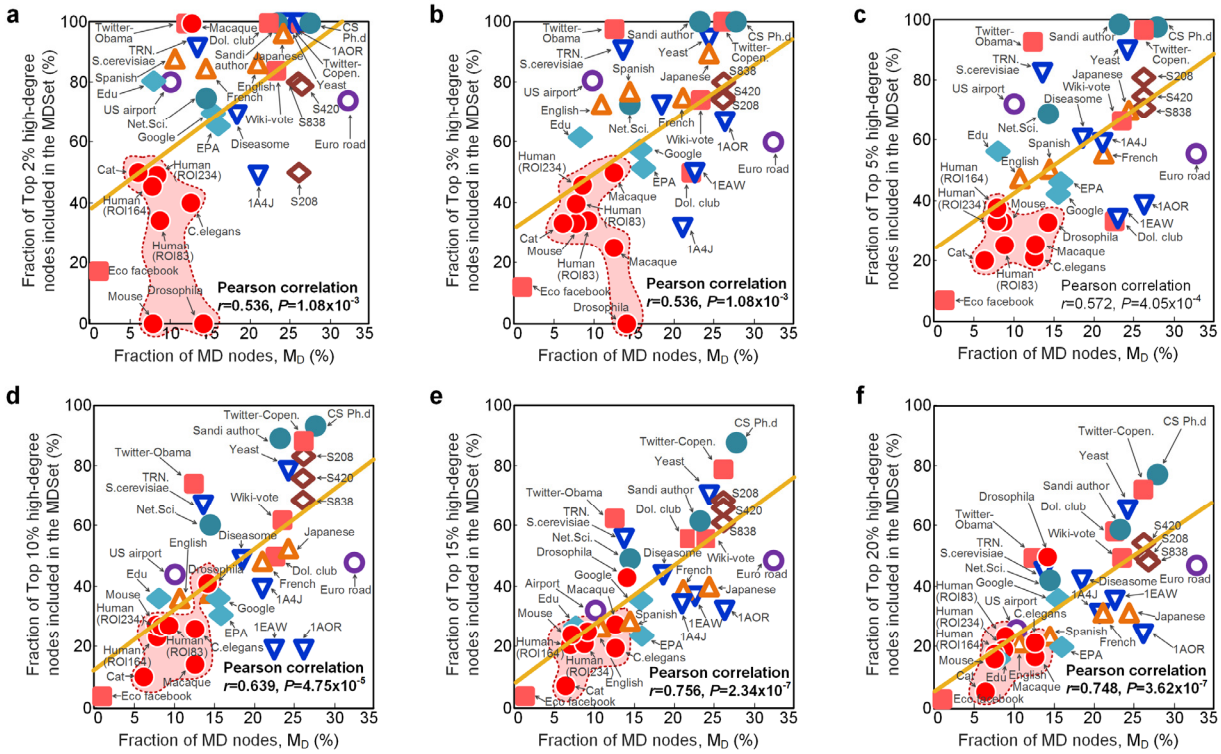

Figure S1. Proportion of high-degree nodes included in the MDSet and its relationship with the fraction of MD-nodes (M_D) in a network. Related to Figure 1. Proportion of high-degree nodes included in the MDSet was examined for top **(A)** 2%, **(B)** 3%, **(C)** 5%, **(D)** 10%, **(E)** 15%, and **(F)** 20% high-degree nodes in each network.

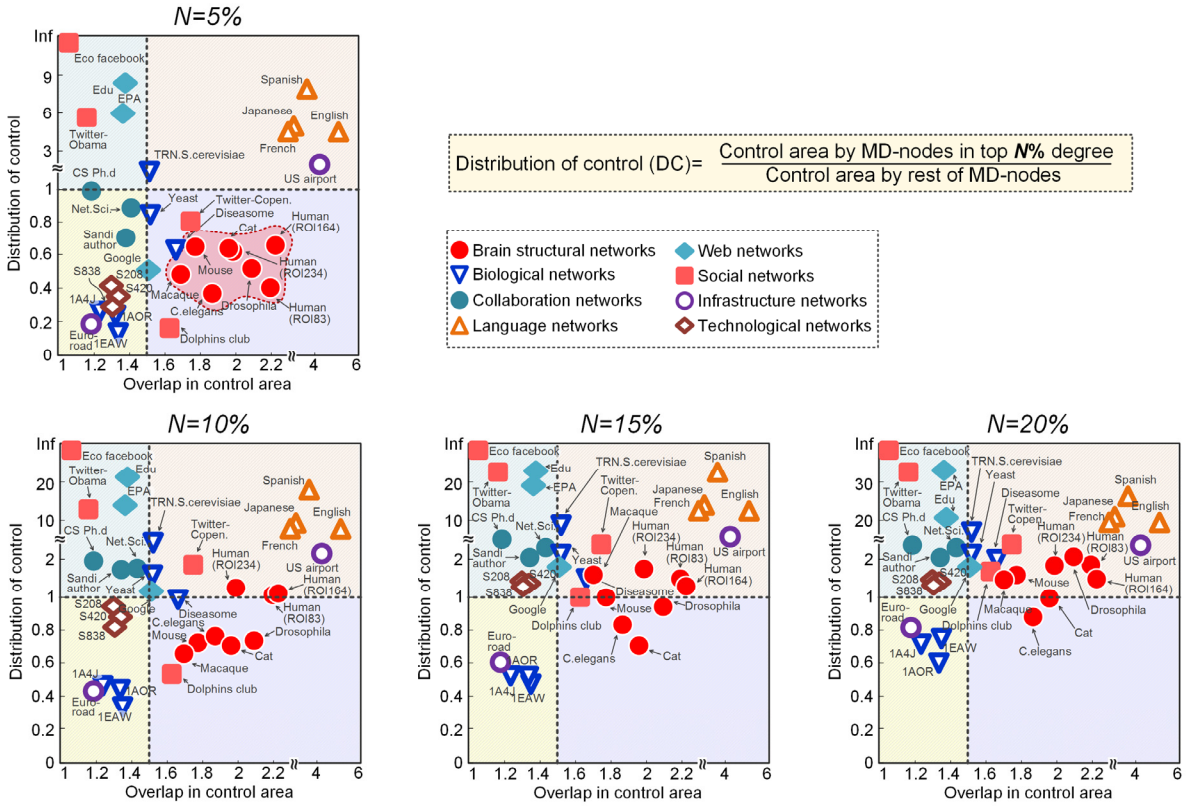

Figure S2. Changes in networks' control architectures depending on the distribution of control (DC) measure. Related to Figure 2. The measure distribution of control (DC) is defined as the ratio between the control area dominated by the MD-nodes in the top N% high-degree nodes and that dominated by the rest of MD-nodes. Control architectures of the networks were examined over N of 5% to 10%, 15%, and 20%.

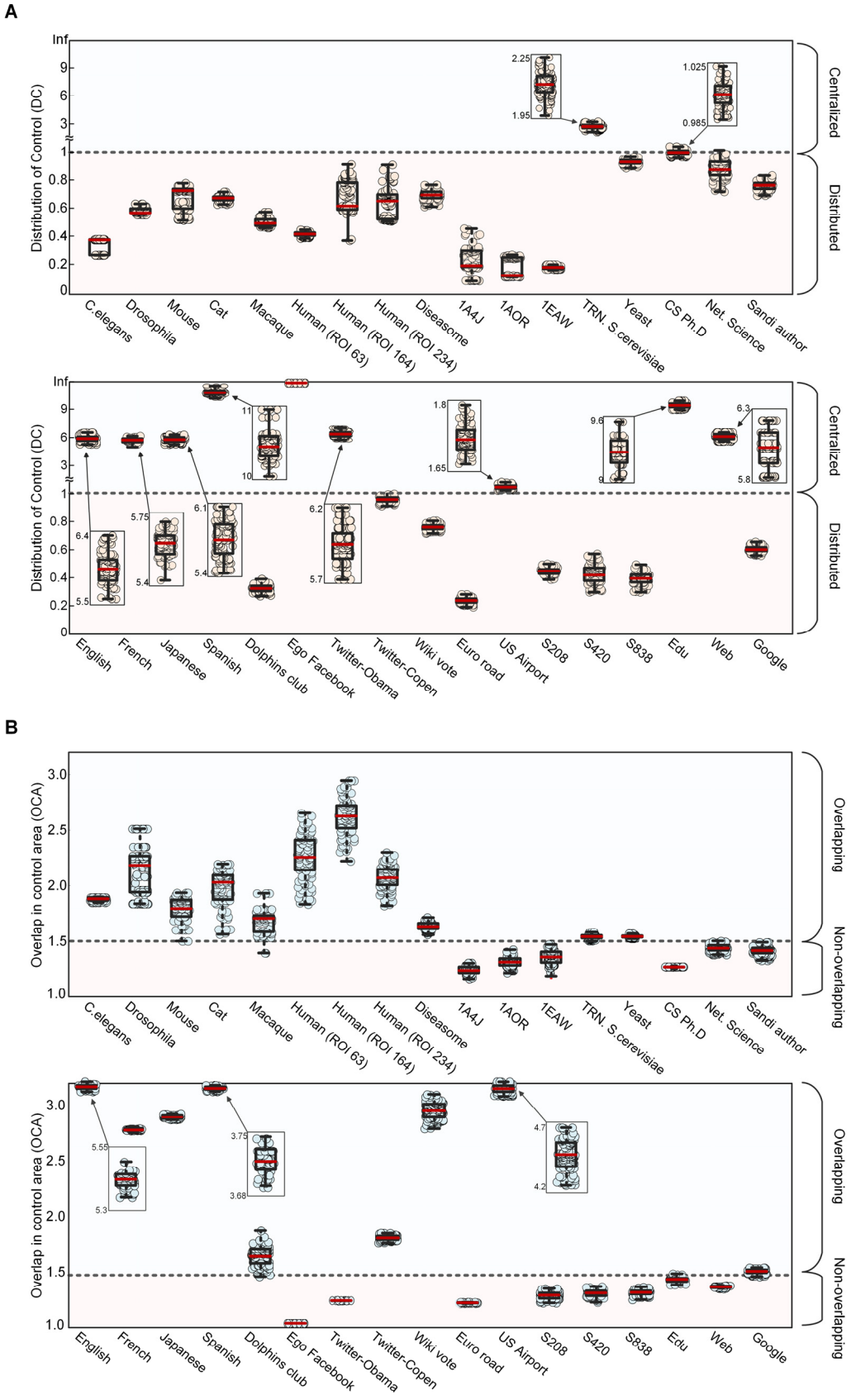

Figure S3. Robustness of *distribution of control (DC)* value and *overlap in control area (OCA)* value against different MDSets in a network. Related to Figure 2. For a given network, the

minimum dominating set (MDSet) may not be unique. For this purpose, we determined 100 MDSets for each network and computed *DC* and *OCA* values of corresponding MDSets. **(A)** We examined how the different choices of MDSet affect the network's *distribution of control (DC)* value, which determines whether the network will follow a *centralized* or *distributed* control architecture. ($DC > 1$: centralized, $DC \leq 1$: distributed). **(B)** We examined how the different choices of MDSet affect the network's *overlap in control area (OCA)* value, which determines whether the network will follow an *overlapping* or *non-overlapping* control architecture ($OCA > 1.5$: overlapping, $OCA \leq 1.5$:non-overlapping).

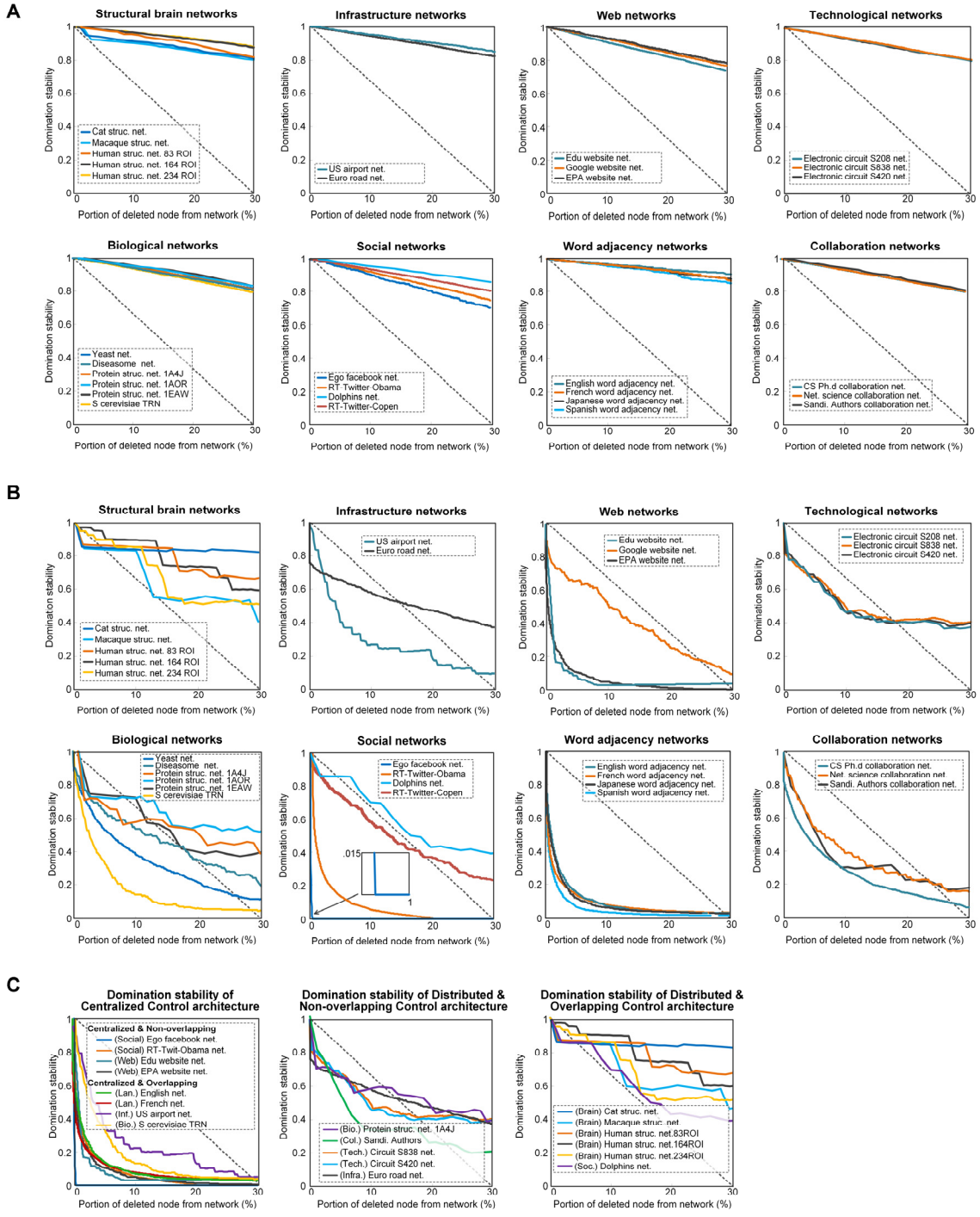

Figure S4. Domination stabilities of various networks against random and targeted attacks. Related to Figure 2. (A) Disruption of control area along with random attacks was monitored for each network. Random attacks were performed by removing random nodes with equal probability in a random order. Random attacks were repeated for 1,000 times, and each plot shows an averaged domination stability of each network. **(B)** Disruption of control area along with targeted attacks was monitored for each network. Targeted attacks were carried out by sequentially removing highest degree nodes. **(C)** Domination stabilities of various networks

against the targeted attacks were reorganized according to their underlying control architectures.

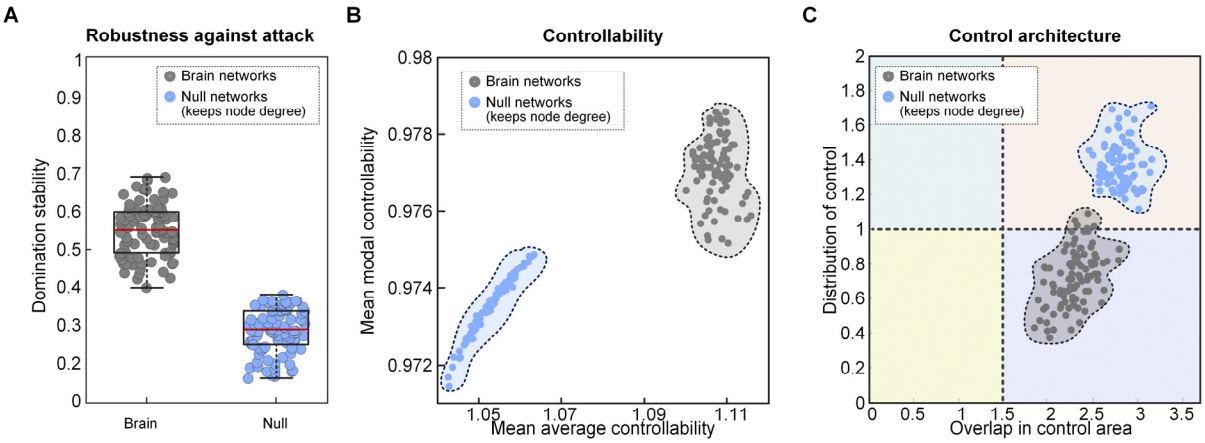

Figure S5. Comparison of robustness and controllability of brain networks with those of random null networks. Related to Figure 4. We generated random null networks derived from human brain networks and examined their robustness (measured by domination stability against targeted attack of top 20% high-degree nodes), controllability (measured by average controllability and modal controllability), and the characteristics of control architecture. **(A, B)** We found that the random null networks have much lower robustness and controllability than the brain networks. **(C)** Random null networks have a *centralized and overlapping* control architecture while the brain networks have a *distributed and overlapping* control architecture.

Supplemental Tables

Table S1. Information of networks analyzed in this study. Related to Figure 1 and Figure 2. For each network, we show its type and name; number of nodes (*N*); fraction of MD nodes (M_D); fraction of top 5% high-degree nodes included in the MDSet (*degree concentration*); distribution of control (*DC*) and overlap in control area (*OCA*); mean average controllability (Con_{Avg}) and mean modal controllability (Con_{Mod}).

Type	Name	*N*	M_D	*Degree concentration*	*DC*	*OCA*	Con_{Avg}	Con_{Mod}
Brain	C.elegans network	272	0.127	0.214	0.345	1.878	1.061	0.974
	Drosophila network	49	0.143	0.333	0.579	2.136	1.160	0.962
	Mouse structural network	112	0.080	0.333	0.670	1.781	1.131	0.969
	Cat structural network	95	0.063	0.200	0.682	1.981	1.120	0.977
	Macaque structural network	71	0.127	0.250	0.506	1.677	1.096	0.962
	Human structural network (ROI 83)	83	0.090	0.250	0.413	2.251	1.157	0.959
	Human structural network (ROI 164)	164	0.079	0.375	0.669	2.614	1.102	0.977
	Human structural network (ROI 234)	234	0.085	0.333	0.628	2.069	1.089	0.971
Biological	Diseasome network	516	0.186	0.613	0.706	1.642	1.046	0.974
	Protein structure 1A4J	95	0.211	0.600	0.236	1.246	1.182	0.889
	Protein structure 1AOR	99	0.263	0.400	0.146	1.313	1.127	0.924
	Protein structure 1EAW	53	0.226	0.337	0.192	1.351	1.169	0.899
	S.cerevisiae transcription network	688	0.137	0.834	2.100	1.539	1.037	0.977
	Yeast network	1458	0.242	0.904	0.962	1.542	1.051	0.963
Collaboration	CS. Ph.D. collaboration	1882	0.228	0.983	1.010	1.264	1.038	0.976
	Network science collaboration	379	0.145	0.694	0.892	1.436	1.057	0.963
	Sandi authors collaboration	86	0.233	1.000	0.776	1.402	1.139	0.912

Table S1: Continuation of Supplementary Table 1.

Type	Name	*N*	M_D	*Degree concentration*	*DC*	*OCA*	Con_{Avg}	Con_{Mod}
Language	Word adjacency (English)	7724	0.108	0.466	5.946	5.417	1.008	0.999
	Word adjacency (French)	9424	0.212	0.548	5.601	2.779	1.005	0.998
	Word adjacency (Japanese)	3177	0.243	0.691	5.769	2.891	1.009	0.997
	Word adjacency (Spanish)	12642	0.146	0.496	10.408	3.721	1.005	0.999
Social	Dolphins club	62	0.226	0.333	0.306	1.634	1.095	0.938
	Ego Facebook	2888	0.003	0.069	Inf	1.308	1.015	0.998
	Obama twitter retweet	3212	0.126	0.929	5.920	1.242	1.015	0.993
	Copenhagen retweet	761	0.261	0.968	0.959	1.796	1.036	0.973
Infra-structur	Euro road	1174	0.327	0.553	0.236	1.222	1.125	0.904
	US 500 busiest airport	500	0.102	0.724	1.705	4.455	1.051	0.995
Technological	Electronic circuit S208	122	0.263	0.809	0.439	1.286	1.171	0.881
	Electrical circuit S420	252	0.262	0.746	0.425	1.303	1.155	0.889
	Electrical circuit S838	512	0.262	0.710	0.391	1.314	1.117	0.911
Web	Educational institute website	3031	0.082	0.568	9.275	1.428	1.009	0.995
	EPA website	4772	0.159	0.463	6.135	1.360	1.017	0.988
	Google website	1299	0.158	0.424	0.605	1.502	1.020	0.988

Table S2. Association of the highly selected MD-nodes to cognitive systems. Related to Figure 3. We identified MDSets from brain networks of 100 healthy adult subjects, composed of 164 cortical and subcortical regions extracted from the Destrieux atlas (Fischl et al., 2004). Then, we identified highly selected (more than 60%) MD-nodes across 100 subjects. Consequently, 12 nodes were chosen as the highly selected MD-nodes. We associated each MD-node to cognitive systems, which are previously defined in the literature: default-mode, sensorimotor, auditory, visual, dorsal attention, ventral attention, fronto-parietal, and subcortical systems.

Position (L: left, R: right)	Node (region) name	Association to cognitive system	Cognitive system assignment
(L, R)	Inferior frontal gyrus	Triangular part of the inferior frontal gyrus is associated with the front-parietal network(Coull et al., 1996; Sturm et al., 1999).	Frontoparietal system
(L, R)	Superior frontal gyrus	The superior frontal cortex is predominantly affiliated with the default mode system (Garrity et al., 2007; Power et al., 2011; Watanabe et al., 2013).	Default-mode system
(L)	Fusiform gyrus	The fusiform gyrus forms a visual system (Agam et al., 2010; Bölte et al., 2006; Power et al., 2011; Xu et al., 2014).	Visual system
(L)	Superior parietal gyrus	The superior parietal cortex plays a crucial role in both the sensorimotor system(Fabbri et al., 2014) and the dorsal attention system(Sestieri et al., 2013; Xu et al., 2014).	Sensorimotor & dorsal attention system
(L, R)	Superior temporal gyrus	The superior temporal gyrus plays a central role in both the auditory system(Woods and Alain, 2009) and the ventral attention system(Corbetta et al., 2005).	Auditory system & ventral attention system
(L, R)	Sulcus of corpus callosum	The corpus callosum is predominantly associated with the default mode system(Garrity et al., 2007).	Default-mode system
(L, R)	Putamen	The putamen is predominantly associated with the subcortical system(Karnath et al., 2002).	Subcortical system

Transparent Methods

Brain network construction

In this study, structural brain networks representing anatomical connections (i.e., edges) between brain regions (i.e., nodes) were constructed from the structural and diffusion magnetic resonance imaging (MRI) data obtained from the Human Connectome Project (HCP) database. The HCP scanning protocol was approved by the local Institutional Review Board at Washington University in St. Louis. We constructed brain networks of 100 healthy human adults by using the preprocessed structural and diffusion dataset of *100 unrelated subjects* from the *HCP 1200 Subject Release* (https://db.humanconnectome.org). Full details of the preprocessing pipeline can be found from (Glasser et al., 2013). Brain network construction was performed through the following processes using MRtrix (Tournier et al., 2012). Specifically, by using structural MRI data, the brain was parcellated into 164 cortical and subcortical regions extracted from the Destrieux atlas (Fischl et al., 2004). Parcellated regions were determined as nodes in the network. In the next, the inter-regional connections (i.e., fiber tracts) were identified using the diffusion MRI data. This step consists of two sub-processes: (1) calculation of the fiber orientation density (FOD) by utilizing constrained spherical deconvolution (CSD) (Tournier et al., 2004) and (2) tracing white-matter fiber tracts by using the probabilistic tractography algorithm (Jbabdi and Johansen-Berg, 2011). In this study, 10 million tracts were traced using anatomically constrained tractography (ACT) (Smith et al., 2012) with the default settings of MRtrix (Tournier et al., 2012). Finally, the adjacency matrix was obtained by counting the number of fiber tracts connecting each pair of regions.

To determine a minimum dominating set (MDSet) from each of the reconstructed networks, we represented each network in a binary fashion by setting connection between region i and j to 1 if a streamline between i and j exists and zero otherwise. To compare with other real-world complex networks (for **Figures 1D, E** and **Figures 2B, C, D**), we reconstructed a group-averaged structural brain network of 100 individual subjects by selecting all connections that were present in at least 75% of the 100 subjects.

Network collection

For comparison, structural brain networks of human at different scale and those of other species (Caenorhabditis elegans, drosophila, mouse cat and macaque) were collected. Structural brain networks of the same 100 human adult subjects parcellated into 83 and 234 regions (subdivided by Lausanne atlas (Hagmann et al., 2008)) were collected from the *Budapest Reference Connectome Server v2.0* (Szalkai et al., 2015), and we further reconstructed a group-averaged network for each parcellation scheme. Structural brain networks of cat and macaque were collected from the Brain Connectivity Toolbox website (https://sites.google.com/site/bctnet/). Lastly, structural brain networks of mouse, C.elegans, and drosophila were collected from the NeuroData's Graph DataBase (https://neurodata.io/project/connectomes/). In addition to collecting structural brain networks, we collected 26 complex networks from 7 disparate fields, ranging from biological

networks and social networks to technological networks and various other types of complex networks. These were collected from the Uri Alon's website (http://www.weizmann.ac.il/mcb/UriAlon/) and the Network Repository website (https://toreopsahl.com/datasets/). Details of each network are summarized in **Table S1.**

Determination of a minimum dominating set

A subset of nodes $D \subseteq V$ in a network $G = (V, E)$ is defined as the dominating set if every node $v \in V$ is either an element of D or connected to at least one element of D. The smallest dominating set for a network G is defined as the minimum dominating set (MDSet), and we used the binary integer programming to determine the MDSet in a network (Nacher and Akutsu, 2013, 2014; Wuchty, 2014). In particular, we used the branch-and-bound algorithm(Land and Doig, 1960) in *lpSolve* library of the programming language R to solve the binary integer-programing problem. Determination of MDSet was performed by finding $min \sum_{v \in V} x_v$, with the constraint $x_v + \sum_{w \in \Gamma(v)} x_w \geq 1$, where $\Gamma(v)$ is the set of one-step neighbors of node v.

Categorization of control architecture

To characterize the underlying control architecture of a network, we defined two measures to determine the interdependence of the control areas dominated by the MD-nodes: *distribution of control* and *overlap in control area*. The *distribution of control* is defined as the ratio between the control area dominated by the MD-nodes in top 5% high-degree nodes and that dominated by the rest of MD-nodes. The distribution of control, DC, is given by

$$DC = \frac{|U_{i \in MDSet\_top} C(i)|}{|U_{i \in MDSet\_bottom} C(i)|}, \quad (1)$$

where $MDSet\_top$ is the subset of MDSet, consisting of the MD-nodes in top 5% high-degree-nodes in a network, $MDSet\_bottom$ is the subset of MDSet, consisting of the MD-nodes in rest of 95% nodes in a network, and $C(i)$ is the set of nodes dominated by the dominating-node i. The control area is defined as the number of nodes dominated by dominating-node i, i.e., $|C(i)|$. We defined that the control architecture of a network is a *centralized* architecture if $DC > 1$ and a *distributed* architecture if $DC \leq 1$. The *overlap in control area* is defined as the degree of overlap between control areas dominated by MD-nodes. The *overlap in control area*, OCA, is given by

$$OCA = \frac{\sum_{i=1}^{M} |C(i)|}{N}, \quad (2)$$

where N is the number of nodes in the network and M is the number of MD-nodes in a MDSet. We defined that the control architecture of a network is an *overlapping* architecture if $OCA > 1.5$ and a *non-overlapping* architecture if $OCA \leq 1.5$. Using *distribution of control* and *overlap in control area*, we categorized the control architecture of a network into the following four distinct types: *centralized and overlapping*, *centralized and non-overlapping*, *distributed and overlapping*, and *distributed and non-overlapping* control architectures.

Domination stability

The disruption of control areas along with the network damage was measured by *domination stability* (Molnár Jr et al., 2015), which is given by

$$DS(f) = \frac{|U_{i \in DSet} C^{+}(i)|}{N-f}, \quad (3)$$

where N is the number of nodes in the network, f is the number of nodes removed from the network, $DSet$ is the subset of the original MDSet that remains after network damage, and $C^{+}(i)$ is the set of nodes still dominated by the dominating-node i after network damage.

We considered two attack scenarios: random attacks and targeted attacks. Random attacks were performed by removing nodes randomly with equal probability in a random order (see **Figure S4A** for the domination stability of each network against random attacks). On the other hand, targeted attacks were performed by removing highest degree nodes sequentially (see **Figure 2C** and **Figure S4B** and **Figure S4C** for the domination stability of each network against targeted attacks).

Average controllability versus modal controllability

Controllability of a network means the capability of driving a network state, defined as a set of node activities, into another one by an external control input (Klamka, 1963). Let us consider the following linear discrete-time and time-invariant model as in study by Gu *et al.* (Gu et al., 2015):

$$\boldsymbol{x}(t+1) = \boldsymbol{A}\boldsymbol{x}(t) + \boldsymbol{B}_{\mathcal{K}}\boldsymbol{u}_{\mathcal{K}}(t), \quad (4)$$

where $\boldsymbol{x}$ is the state of brain network over time, $\boldsymbol{A}$ is the binarized structural connectivity matrix of brain derived from tractography data, $\boldsymbol{B}_{\mathcal{K}}$ is the input matrix that identify the control points, and $\boldsymbol{u}_{\mathcal{K}}$ is the control strategy.

Previous results in control theory guarantee that controllability of a network in Eq. (4) by the set of control nodes $\boldsymbol{\mathcal{K}}$ is equivalent to the controllability Gramian $\boldsymbol{W}_{\mathcal{K}}$ being invertible, where

$$W_{\mathcal{K}} = \sum_{\tau=0}^{\infty} A^{\tau} B_{\mathcal{K}} B_{\mathcal{K}}^{\mathrm{T}} A^{\tau}, \quad (5)$$

We adopted this framework to select control nodes one at a time, resulting in reducing the input matrix B to a one-dimensional vector.

We examined two different control strategies: *average controllability* and *modal controllability* (Gu et al., 2015). Average controllability of a network is identical to the average input energy from $\mathcal{K}$ (i.e., a set of control nodes) and over all possible target states. Following the study by Gu *et al*. (Gu et al., 2015), we used Trace ($W_{\mathcal{K}}$) as a measure for the average controllability. Nodes with high average controllability are known to be most influential for controlling a network over all nearby target states with the least amount of input energy. Modal controllability is computed from the eigenvector matrix $V = [v_{ij}]$ of the structural connectivity matrix **A**. Modal controllability of node i is defined as $\phi_i = \sum_{j=1}^{N}(1 - \lambda_j^2(A))\lambda_{ij}^2$, providing a measure of the controllability to all *N* modes $\lambda_1(A), \ldots, \lambda_N(A)$ from the node i (see the study by Gu *et al.* (Gu et al., 2015) for details). Nodes with high modal controllability can drive a network state into the difficult-to-reach distant state.

In this study, we used the MATLAB codes downloaded from Danielle Bassett's website (https://www.danisbassett.com) to compute average and modal controllability of various networks. Our major interest was comparing controllability of various networks rather than analyzing controllability of particular nodes in a specific network. So, to investigate the overall controllability of a network, we examined the mean average controllability and mean modal controllability that are computed by averaging the average controllability and modal controllability, respectively, of all nodes.

Graph theoretical analysis

All graph theoretical analyses were performed using the Brain Connectivity Toolbox (http://sites.google.com/site/bctnet/).

Rich club detection

Rich club (RC) nodes are a group of high-degree nodes that are densely interconnected beyond the expectation. Detection of RC-nodes was performed over a range of degrees. For degree k, nodes with degree $\leq k$ were eliminated from the network and the RC coefficient $\phi(k)$, which is defined as the ratio of existing connections to all possible connections, was computed. Then, $\phi(k)$ was simultaneously normalized to the averaged RC coefficient over 1,000 random networks with a preserved degree distribution. The normalized RC coefficient, $\phi_{norm}(k) = \phi(k)/\phi_{random}(k)$, that exceeds one suggests the existence of a set of RC-nodes of degree k. This procedure was repeated over a larger degree than k. To examine the correspondence between MD-nodes and RC-nodes (**Figure 3B** and **3C**), we detected a set of RC-nodes from each structural brain network that matches the size of the MDSet determined from the same network. We confirmed that ϕ_{norm} of the detected set of nodes in each network is greater than one, satisfying the aforementioned condition for being RC-nodes.

Computation of transitivity

Transitivity determines the prevalence of clustered connectivity in a network. Transitivity of a network is given by

$$T = \frac{\sum_{i \in N} 2t_i}{\sum_{i \in N} k_i(k_i - 1)}, \quad (6)$$

where N is the number of nodes in the network, t_i is the number of triangles around a node i, and k_i is the degree of node i. In this study, we explored the relationship between MD-nodes and the network transitivity by deleting MD-nodes from the networks. Transitivity of a network is known to be strongly influenced by provincial hubs and connector hubs, where deleting provincial hubs decreases the transitivity of a network while deleting connector hubs produces the opposite effect (Sporns et al., 2007). By examining the change of transitivity in the network after deletion of MD-nodes, we determined whether the MD-nodes are primarily provincial hubs or connector hubs.

Module detection and participation coefficient

To examine the modularity of structural brain networks and the role of MD-nodes in interconnecting modules, we performed module partitioning on each structural brain network using the Louvain community detection algorithm (Blondel et al., 2008). MD-nodes were further classified into provincial hubs and connector hubs based on their level of participation to the local module connection or between module connection. The level of intra-module connectivity versus inter-module connectivity of a node can be determined by the *participation coefficient* of the node(Rubinov and Sporns, 2010). Formally, *participation coefficient* of node i, PC_i, is defined as

$$PC_i = 1 - \sum_{m=1}^{N_m} \left(\frac{k_{im}}{k_i}\right)^2, \quad (7)$$

where N_m is the number of modules, k_i is the degree of node i, and k_{im} is the number of connections from node i to module m. Following the study by Heuvel *et al.* (Van Den Heuvel and Sporns, 2011), we defined node i as a provincial hub if $PC_i \leq 0.5$ and connector hub otherwise.

Artificial network evolution based on Pareto optimization

For artificial network evolution analysis, we generated 100 random null networks derived from 100 structural human brain networks composed of 164 nodes. The random null networks were generated using the function *randmio_und_connected* in the Brain Connectivity Toolbox, which randomly permutes the edges of a network while preserving the number of nodes and degree distribution.

Starting from the generated random null networks, we performed 500 epochs of network evolution on each network in the direction of improving the following three objective functions: domination stability against targeted attack of top 20% high-degree nodes, mean average controllability, and mean modal controllability. We employed an evolutionary algorithm called Pareto optimization (Holland and Goldberg, 1989), which has been used in previous studies to explore brain network topology (Avena-Koenigsberger et al., 2014; Tang et al., 2017). Pareto optimization was performed by repeatedly carrying out the following two steps in each evolutionary epoch: network variation and network selection. Network variation was performed by employing a rewiring algorithm called 'edge-swaps' (Avena-Koenigsberger et al., 2014; Coolen et al., 2009) which randomly choose an existing edge in a network and replace it with an edge that did not previously exist. Such edge-swapping was performed to generate 100 networks with differently rewired edges. Network selection was performed by evaluating three features (i.e., domination stability, average controllability, and modal controllability) for all the 100 edge-rewired networks according to Pareto optimality (Holland and Goldberg, 1989). A network that advances the Pareto front (Petrie et al., 1995) most (i.e., advances the three objective functions most) was selected and the next evolutionary epoch was performed with the selected network. During the evolutionary process, all networks were kept to preserve the number of nodes, edges, and degree distribution.

Reference

Agam, Y., Liu, H., Papanastassiou, A., Buia, C., Golby, A.J., Madsen, J.R., and Kreiman, G. (2010). Robust selectivity to two-object images in human visual cortex. Current Biology *20*, 872-879.

Avena-Koenigsberger, A., Goñi, J., Betzel, R.F., van den Heuvel, M.P., Griffa, A., Hagmann, P., Thiran, J.-P., and Sporns, O. (2014). Using Pareto optimality to explore the topology and dynamics of the human connectome. Phil Trans R Soc B *369*, 20130530.

Blondel, V.D., Guillaume, J.-L., Lambiotte, R., and Lefebvre, E. (2008). Fast unfolding of communities in large networks. Journal of statistical mechanics: theory and experiment *2008*, P10008.

Bölte, S., Hubl, D., Feineis-Matthews, S., Prvulovic, D., Dierks, T., and Poustka, F. (2006). Facial affect recognition training in autism: can we animate the fusiform gyrus? Behavioral neuroscience *120*, 211.

Coolen, A., De Martino, A., and Annibale, A. (2009). Constrained Markovian dynamics of random graphs. Journal of Statistical Physics *136*, 1035-1067.

Corbetta, M., Kincade, M.J., Lewis, C., Snyder, A.Z., and Sapir, A. (2005). Neural basis and recovery of spatial attention deficits in spatial neglect. Nature neuroscience *8*, 1603.

Coull, J., Frith, C., Frackowiak, R.S.J., and Grasby, P. (1996). A fronto-parietal network for rapid visual information processing: a PET study of sustained attention and working memory. Neuropsychologia *34*, 1085-1095.

Fabbri, S., Strnad, L., Caramazza, A., and Lingnau, A. (2014). Overlapping representations for grip type and reach direction. Neuroimage *94*, 138-146.

Fischl, B., Van Der Kouwe, A., Destrieux, C., Halgren, E., Ségonne, F., Salat, D.H., Busa, E., Seidman, L.J., Goldstein, J., and Kennedy, D. (2004). Automatically parcellating the human cerebral cortex. Cerebral cortex *14*, 11-22.

Garrity, A.G., Pearlson, G.D., McKiernan, K., Lloyd, D., Kiehl, K.A., and Calhoun, V.D. (2007). Aberrant "default mode" functional connectivity in schizophrenia. American journal of psychiatry *164*, 450-457.

Glasser, M.F., Sotiropoulos, S.N., Wilson, J.A., Coalson, T.S., Fischl, B., Andersson, J.L., Xu, J., Jbabdi, S., Webster, M., and Polimeni, J.R. (2013). The minimal preprocessing pipelines for the Human Connectome Project. Neuroimage *80*, 105-124.

Gu, S., Pasqualetti, F., Cieslak, M., Telesford, Q.K., Alfred, B.Y., Kahn, A.E., Medaglia, J.D., Vettel, J.M., Miller, M.B., and Grafton, S.T. (2015). Controllability of structural brain networks. Nature communications *6*, 8414.

Hagmann, P., Cammoun, L., Gigandet, X., Meuli, R., Honey, C.J., Wedeen, V.J., and Sporns, O. (2008). Mapping the structural core of human cerebral cortex. PLoS biology *6*, e159.

Holland, J., and Goldberg, D. (1989). Genetic algorithms in search, optimization and machine learning. Massachusetts: Addison-Wesley.

Jbabdi, S., and Johansen-Berg, H. (2011). Tractography: where do we go from here? Brain connectivity *1*, 169-183.

Karnath, H.O., Himmelbach, M., and Rorden, C. (2002). The subcortical anatomy of human spatial neglect: putamen, caudate nucleus and pulvinar. Brain *125*, 350-360.

Klamka, J. (1963). Controllability of linear dynamical systems.

Land, A.H., and Doig, A.G. (1960). An automatic method of solving discrete programming problems. Econometrica: Journal of the Econometric Society, 497-520.

Molnár Jr, F., Derzsy, N., Szymanski, B.K., and Korniss, G. (2015). Building damage-resilient dominating sets in complex networks against random and targeted attacks. Scientific reports *5*, 8321.

Nacher, J.C., and Akutsu, T. (2013). Structural controllability of unidirectional bipartite networks. Scientific reports *3*, 1647.
Nacher, J.C., and Akutsu, T. (2014). Analysis of critical and redundant nodes in controlling directed and undirected complex networks using dominating sets. Journal of Complex Networks *2*, 394-412.
Petrie, C.J., Webster, T.A., and Cutkosky, M.R. (1995). Using Pareto optimality to coordinate distributed agents. AI EDAM *9*, 269-281.
Power, J.D., Cohen, A.L., Nelson, S.M., Wig, G.S., Barnes, K.A., Church, J.A., Vogel, A.C., Laumann, T.O., Miezin, F.M., and Schlaggar, B.L. (2011). Functional network organization of the human brain. Neuron *72*, 665-678.
Rubinov, M., and Sporns, O. (2010). Complex network measures of brain connectivity: uses and interpretations. Neuroimage *52*, 1059-1069.
Sestieri, C., Capotosto, P., Tosoni, A., Romani, G.L., and Corbetta, M. (2013). Interference with episodic memory retrieval following transcranial stimulation of the inferior but not the superior parietal lobule. Neuropsychologia *51*, 900-906.
Smith, R.E., Tournier, J.-D., Calamante, F., and Connelly, A. (2012). Anatomically-constrained tractography: improved diffusion MRI streamlines tractography through effective use of anatomical information. Neuroimage *62*, 1924-1938.
Sporns, O., Honey, C.J., and Kötter, R. (2007). Identification and classification of hubs in brain networks. PloS one *2*, e1049.
Sturm, W., De Simone, A., Krause, B., Specht, K., Hesselmann, V., Radermacher, I., Herzog, H., Tellmann, L., Müller-Gärtner, H.-W., and Willmes, K. (1999). Functional anatomy of intrinsic alertness: evidencefor a fronto-parietal-thalamic-brainstem network in theright hemisphere. Neuropsychologia *37*, 797-805.
Szalkai, B., Kerepesi, C., Varga, B., and Grolmusz, V. (2015). The Budapest reference connectome server v2. 0. Neuroscience Letters *595*, 60-62.
Tang, E., Giusti, C., Baum, G.L., Gu, S., Pollock, E., Kahn, A.E., Roalf, D.R., Moore, T.M., Ruparel, K., and Gur, R.C. (2017). Developmental increases in white matter network controllability support a growing diversity of brain dynamics. Nature Communications *8*, 1252.
Tournier, J.-D., Calamante, F., Gadian, D.G., and Connelly, A. (2004). Direct estimation of the fiber orientation density function from diffusion-weighted MRI data using spherical deconvolution. NeuroImage *23*, 1176-1185.
Tournier, J.D., Calamante, F., and Connelly, A. (2012). MRtrix: diffusion tractography in crossing fiber regions. International Journal of Imaging Systems and Technology *22*, 53-66.
Van Den Heuvel, M.P., and Sporns, O. (2011). Rich-club organization of the human connectome. Journal of Neuroscience *31*, 15775-15786.
Watanabe, T., Hirose, S., Wada, H., Imai, Y., Machida, T., Shirouzu, I., Konishi, S., Miyashita, Y., and Masuda, N. (2013). A pairwise maximum entropy model accurately describes resting-state human brain networks. Nature communications *4*, 1370.
Woods, D.L., and Alain, C. (2009). Functional imaging of human auditory cortex. Current opinion in otolaryngology & head and neck surgery *17*, 407-411.
Wuchty, S. (2014). Controllability in protein interaction networks. Proceedings of the National Academy of Sciences *111*, 7156-7160.
Xu, P., Huang, R., Wang, J., Van Dam, N.T., Xie, T., Dong, Z., Chen, C., Gu, R., Zang, Y.-F., and He, Y. (2014). Different topological organization of human brain functional networks with eyes open versus eyes closed. Neuroimage *90*, 246-255.